

This version of the article has been accepted for publication, after peer review (when applicable) and is subject to Springer Nature's AM terms of use(<https://www.springernature.com/gp/open-research/policies/accepted-manuscript-terms>), but is not the Version of Record and does not reflect post-acceptance improvements, or any corrections. The Version of Record is available online at: <http://dx.doi.org/10.1007/s12273-020-0756-5>.

The following publication Gao, Z., Li, S.S., Gao, Y. et al. Numerical studies on swirling of internal fire whirls with experimental justifications. Build. Simul. 14, 1499–1509 (2021) is available at <https://doi.org/10.1007/s12273-020-0756-5>.

## **Experimental and Numerical Studies on Swirling of Internal Fire Whirls**

Z.M. Gao, S.S. Li and Y. Gao  
College of Aerospace and Civil Engineering  
Harbin Engineering University  
Harbin, Heilongjiang, China

H.Y. Hung and W.K. Chow\*  
Department of Building Services Engineering  
The Hong Kong Polytechnic University  
Hong Kong, China

\*Corresponding author:

Fax: (852) 2765 7198; Tel: (852) 2766 5843

Email: [beelize@polyu.edu.hk](mailto:beelize@polyu.edu.hk); [bewkchow@polyu.edu.hk](mailto:bewkchow@polyu.edu.hk)

Postal address: Department of Building Services Engineering, The Hong Kong Polytechnic University, Hunghom, Kowloon, Hong Kong.

December 2017

## Nomenclature

$C_S$	Turbulence SGS Smagorinsky model coefficient
$c_p$	Air specific heat. kg/m <sup>3</sup>
$D_T$	Mass diffusion coefficient
$D^*$	Flame characteristic diameter
$g$	acceleration due to gravity
$k$	Coefficients for centerline correlations
$k_T$	Heat-conductivity factor
$l$	Grid size
$Pr_T$	Turbulent Prandtl number
$Q$	Stable stage HRR
$\bar{Q}$	Mean HRR of six stages
$Q_{in}$	Input stable stage HRR
$\bar{Q}_{in}$	Input mean HRR
$r$	Radial distance from centerline
$Sc_T$	Turbulent Schmidt number
$S_{ij}$	Deformation rate tensor. $i$ for normal direction and $j$ for projective direction.
$T$	Temperature
$T_0$	Ambient air temperature
$u_j$	Velocity components( $u, v, w$ ) along the $x, y, z$ Cartesian coordinate
$Y_i$	Mass fraction of component $i$
$z$	Height from fuel surface

## Greek symbols

$\delta$	Rate of particle nucleation for soot volume fraction
$\mu_T$	Turbulent viscosity coefficient
$\rho$	Density
$\rho_0$	Ambient air density
$\tau_{ij,SGS}$	Viscous stress tensor
$\eta$	Exponent of centerline correlation
$\Omega$	Tangential velocity
$\Delta T$	Excess temperature
$\Delta$	Subgrid length scale
$\Delta x, \Delta y, \Delta z$	Grid spacings along the $x, y, z$ Cartesian coordinate system

## **Abstract**

Internal fire whirls (IFW) with single corner gap generated in a vertical shaft model were investigated by experiments and numerical simulations. IFW generation process, fuel burning rate and temperature history were studied. Typical transient experimental and simulated flame shape deduced from temperature were studied. The dynamic phenomena of IFW generation and development was captured in both methods. Numerical simulations on medium scale IFW using a fully-coupled large eddy simulation incorporating subgrid scale turbulence and a fire source with heat release rates compiled from experimental results were carried out. Validation by comparing predicted results with experimental data demonstrated that an IFW can be simulated by CFD. Experimental and numerical results for flame surface, temperature, and flame length were in good agreement. IFW flame region and intermittent region were longer than ordinary pool fire. The modified centerline temperature empirical formula was derived. Variations of vertical and tangential velocity in axial and radial directions were shown. The vortex core radius was found to be determined by fuel bed size.

**Keywords:** Internal fire whirl, Large eddy simulation, Vertical structure, Flame surface

## 1. Introduction

Fire whirl, due to its intensive combustion, high temperature and heat release rate (HRR), will cause more severe damage than ordinary fire (Soma and Saito, 1991). Generation of fire whirl in laboratory environment was first reported by Emmons and Ying (1996) and Satoh and Yang (1998) more than 2 decades ago. The formation of fire whirl is due to the coupling of upward airflow caused by buoyancy and tangential airflow. Angular momentum was believed to be the key element. Some vertical shaft fire whirl experiments have been done (Satoh and Yang, 1998, 1999; Yu and Guo, 2013) to study the impact of gap width on flame intensity. Recent studies by Zou and Chow (2015) suggested that fire whirl burnt vigorously when the ratio of gap width to wall width was in a certain range. No velocity field of fire whirl was measured or analyzed by their studies. Lei and Liu (2013, 2015) carried out a series of comprehensive experimental investigations with hot-wire anemometers to precisely measure the velocity at key positions. Semi-empirical formula was used by Lei et al. (2017) with the assumption that turbulent fire whirl height could be calculated based on turbulence suppression. By analysing Richardson Number, turbulent fire whirl suppression was attributed to the decrease of mixing length and plume expansion rate. The flame height, heat release rate, average axial velocity and the Richardson number were interrelated. Comparing with fires of the same fuel pool size, turbulence suppression was suggested to be the dominant mechanism of fire whirl elongation rate. Chuah et al. (2009) clarified that flame height was determined by the vortex core diameter. Since the average heat transfer rate to the burning surface varied inversely to the vortex core diameter, smaller vortex core transferred more heat to the fuel surface and led to higher evaporation rate.

Numerical simulation (Liu and Chow, 2002; Ma and Quintiere, 2003) of fire field, for its nearly unlimited data details, is a good addition to experiment. Previous researches (Murakami, 1998; Zhang and Chen, 2000; Jiang and Chen, 2001) have discussed the application of large eddy simulation to fire field computation and good performance has been reported. Satoh and Yang (1997) carried out simulation by using an approximate fire field model and by directly defining total heat load without experimental guideline. Chow et al. (2017) presented a mathematical methods to study the relationship between burning rate and fire whirl height. Moreover, simulation with the  $k-\varepsilon$  turbulent model and commercial software Fluent was presented but relationships between the parameters of fire whirl were not discussed in depth. Experiment and numerical simulation were performed by Snegirev (2004). The authors suggested that standard and modified turbulent model did affect the simulated fire whirl height. Good agreement between experiment and simulation could be obtained when modified turbulent viscosity was utilized. In the numerical simulation, the author got results agreeing with the experimental results by enlarging turbulence suppression. Motivated by these experiences, LES method was used in this paper.

The reliability of the fire field simulation is based on the verification versus experiment. In this paper, medium-scale experimental observations were presented to investigate the features of fire whirl, including fuel burning rate, flame height and temperature. The IFW was divided into six stages from generation to extinction. The Fire Dynamics Simulator (FDS) (McGrattan, 2004; McGrattan and Forney, 2004) was used to simulate the IFW using a fire source with heat release rate (HRR) compiled from experimental data. Taking HRR as FDS input parameters, good agreement between simulated and experimental IFW transient flame surface, flame height,

and temperature were achieved. Furthermore, axial (vertical) and tangential velocity, streamline, velocity vector and vortex core were obtained.

## 2. Experimental Studies

A 2.1 m x 2.1 m square vertical shaft 9 m tall with a corner gap of adjustable width as shown in Fig. 1(a) was constructed. A glass wall of 2.0 m × 1.5 m was installed for observing flame whirling motions. The other walls were made of iron sheets. Gasoline pens of different diameters were put at centre of the floor.

The gap width was set as 0.33 m to provide a strong flame swirling. Thermocouples were put in positions as shown in Fig. 1(b). Different horizontal thermocouple distributions were set for different pool size. Tests for gasoline diameters of 0.2 m, 0.26 m and 0.46 m were labelled as SW-S, SW-M and SW-L. Experimental parameters in these tests and results are shown in Table 1.

As observed in the experiments, there were 6 stages in the IFW from ignition to stable swirling and then extinction, as summarized in Table 2.

- Stage I:  
Behaved as a normal pool fire with gas and air temperature increased.
- Stage II:  
Inclined pool fire with centerline temperature decreased.
- Stage III:  
Transition from a normal pool fire to elongated flame height, swirling observed intermittently with temperature rising rapidly.
- Stage IV:  
Inclined fire whirl rotated around central axis with temperature fluctuating.

- Stage V:  
Straight fire whirl with strong swirling flame and steady temperature measured.
- Stage VI:  
Flame swirling decayed with decreasing flame diameter and height until extinction.

Measured axial and horizontal temperature distributions for the three different fire pools were shown in Fig. 2 and Fig. 3. For smaller fuel pool diameter, stage I and II were longer, which mean that the onset of fire whirl was later than bigger ones. Axial temperature rose up to the highest at the end of the transition stage III and then IFW was formed. Stage IV and stage V alternating existence after IFW generation. By comparing SW-S, SW-M and SW-L, large temperature fluctuations were observed for small pool diameters. Non-uniform density difference due to buoyancy was probably the reason of tangential wind generation. IFW trended to be generated easier with fire source having higher HRR.

The transient fuel mass was measured by an electronic scale placed under the fuel pool and was shown in Fig. 4. As the fuel loss rate fluctuation was small, no significant fluctuation on transient fuel mass was observed. The slope in the time interval (200 s to 250 s) of the three curves would give the stage V burning rate. The negative mass readings occurred at the end of combustion due to hot steam and negative pressure above the fuel tray resulted from high temperature.

### 3. Numerical Simulations

The Computational Fluid Dynamics (CFD) software Fire Dynamics Simulator (FDS) is used to simulate the IFW. The simulation results are compared with the experimental data to validate the selected models. Three simulations are conducted corresponding to the above experiments labeled as SW-S, SW-M and SW-L. Based on experimental results, a fire source which heat release rate varying with time is set up. The finite volume method (FVM) as radiation model, the Large Eddy Simulation (LES) method as turbulent model with Subgrid scale (SGS) turbulence Smagorinsky model are used.

SGS Smagorinsky model has been demonstrated to be successful in studying buoyant flames by Zhou et al. (2001), using a viscous stress  $\tau_{ij,SGS}$  shown below.

$$\tau_{ij,SGS} - \frac{1}{3} \delta_{ij} \tau_{kk,SGS} = 2\mu_T \bar{S}_{ij} \quad (1)$$

where

$$\text{Turbulent viscosity coefficient: } \mu_T = \bar{\rho} (C_s \Delta)^2 (2\bar{S}_{ij} \bar{S}_{ij})^{1/2} \quad (2)$$

$$\text{and deformation rate tensor: } \bar{S}_{ij} = \frac{1}{2} \left( \frac{\partial \bar{u}_i}{\partial x_j} + \frac{\partial \bar{u}_j}{\partial x_i} \right) \quad (3)$$

$$\tau_{ij,SGS} = \mu_T (2\bar{S}_{ij} - \frac{2}{3} \delta_{ij} \bar{S}_{kk}) \quad (4)$$

Then turbulent viscosity coefficient is given by

$$\mu_T = \bar{\rho} (C_s \Delta)^2 |S| = \bar{\rho} (C_s \Delta)^2 \left\{ -\frac{2}{3} (\bar{S}_{kk} \delta_{ij})^2 + 2(\bar{S}_{ij})^2 \right\}^{1/2} \quad (5)$$

The subgrid length  $\Delta$  is expressed as  $\Delta=(\Delta x, \Delta y, \Delta z)^{1/3}$ ,  $C_S$  is taken to be within  $0.1 \sim 0.25$ .

Applying literature results in studying turbulent flow (Warrantz et al. 1996), the species diffusion vector is given by:

$$-\bar{\rho}(\overline{Y_l u_j} - \bar{Y}_l \bar{u}_j) = \frac{\mu_T}{Sc_T} \frac{\partial \bar{Y}_l}{\partial x_j} \quad (6)$$

The heat flux vector is

$$-\bar{\rho}(\overline{T u_j} - \bar{T} \bar{u}_j) = \frac{\mu_T}{Pr_T} \frac{\partial \bar{T}}{\partial x_j} \quad (7)$$

The heat-conductivity factor  $k_T$  and mass diffusion coefficient  $D_T$  are given by:

$$k_T = \frac{\mu_T C_p}{Pr_T} \quad (8)$$

$$\rho D_T = \frac{\mu_T}{Sc_T} \quad (10)$$

Smagorinsky constant  $C_S$ , turbulent Schmidt number  $Sc_T$  and turbulent Prandtl number  $Pr_T$  have to be specified in the Smagorinsky model. According to the results of previous studies,  $C_S$  is not sensitive when the grid is small enough (Liu and Chow, 2002). The value of  $C_S$  has an impact on the simulation results when buoyancy is strong. A greater  $C_S$  is recommended (Zhang et al., 2002) when the grids are not fine enough. Values of  $Sc_T$  and  $Pr_T$  have little effect on simulation results. FDS numerical simulation applying SGS model for ordinary pool fire was conducted by Sherman ) (Cheung and Yeoh, 2009) by taking  $C_S=0.2$ ,  $Pr_T=0.7$ ,  $Sc_T=0.3$ . Combining studies by Murakami (1998), Zhang and Chen (2000) and Jiang and Chen (2001),  $C_S=0.2$ ,  $Pr_T=0.5$ ,  $Sc_T=0.5$  are used in this paper.

Uniform Cartesian coordinate grids are used. In order to exactly capture the fire whirl details such as vortex, the grid size is determined by the flame characteristic diameter  $D^*$  and grid size  $l$ .  $D^*/l$  can be seen as the amount of grid in characteristic length. Reasonable results are obtained when  $D^*/l$  lies between 4 and 16 (Jiang and Chen (2001) with  $D^*$  given by:

$$D^* = \left( \frac{\bar{Q}}{\rho_0 c_p T_0 \sqrt{g}} \right)^{\frac{2}{5}} \quad (11)$$

Characteristic diameter  $D^*$  should cover (Wang, 2009) at least 10 grids to capture the fire plume. Taking  $\rho_0 = 1.293 \text{ kg/m}^3$ ,  $c_p = 1.004 \text{ kJ/kg} \cdot \text{K}$ ,  $g = 9.8 \text{ kg/s}^2$ , the calculated grid size is shown in Table 3.

For simulating SW-L, the selected grid size is  $0.05 \text{ m} \times 0.05 \text{ m} \times 0.05 \text{ m}$ . The total number of grids is  $42 \times 42 \times 183$ . For SW-S and SW-M, a smaller grid size of  $0.03 \text{ m}$  was needed to capture flame data. If the grid size of the whole simulation zone is set to be  $0.03 \text{ m} \times 0.03 \text{ m} \times 0.03 \text{ m}$ , the total number of grids is nearly 1.5 million.

The whole computing domain is then divided into several parts to achieve simulated results. A region of  $0.9 \text{ m} \times 0.9 \text{ m} \times 6.0 \text{ m}$  around the flame is set as the flame zone, where  $0.03 \text{ m} \times 0.03 \text{ m} \times 0.03 \text{ m}$  grid is used. The other region is set as the flame far field, where  $0.05 \text{ m} \times 0.05 \text{ m} \times 0.05 \text{ m}$  grid is used. The total number of grids is 0.46 million and the grid setting is shown in Fig. 5. Free boundary conditions on the gap and roof are set to allow fluid flowing across. The velocity and temperature gradients at these boundaries are set to zero.

The estimated total HRR of these three experiments at IFW stable stage are  $\bar{Q} = 125.1$  kW, 213.4 kW, and 552 kW, respectively, higher than the mean HRR over the six stages denoted by  $\bar{Q}$  (in kW). The simulated input stable-stage HRR  $\bar{Q}_{in}$  (in kW) should be equal to  $\bar{Q}$ . Meanwhile, the input mean HRR  $\bar{Q}_{in}$  should be equal to  $\bar{Q}$  (obtained from average fuel loss rate in Fig. 6) too. After stage IV, a stable fire whirl formed. The end time of stage IV is the end of the ascent of the input HRR curve. When the stage VI begins, the fire whirl starts to extinguish, and the IFW is no more stable with the HRR curve starts to decrease,  $\bar{Q}_{in} = \bar{Q}$ . In this way, one can find that the mean input HRR is  $\bar{Q}_{in} = 99.5$  kW, 168 kW and 440.5 kW, very close to estimated mean HRR  $\bar{Q} = 103.4$  kW, 173 kW and 441.6 kW.

Predicted flame temperature, flame height and flame pattern are compared with experimental results first to validate the simulation method using FDS. Flame axial velocity and tangential velocity are then studied by CFD-FDS.

#### 4. Flame Surface and Streamline

Simulation results on the central lateral plane of the shaft under different parameters for SW-L are shown in Fig. 7. The IFW length is 3.1 m. The temperature distribution in Fig. 7(a) shows that the transient IFW temperature is not continuous while the pressure distribution is continuous (Fig. 7(b)). In Fig. 7(c) and Fig. 7(d), the velocity on the centerline and  $v$  at the lower part is smaller than the other regions in IFW. The vertical velocity  $w$  is shown in Fig. 7(e).

Stable strong fire whirl could be generated in the simulation of the three cases corresponding to SW-S, SW-M and SW-L. The flame height has been defined by Zukoski et al. (1981) to be the region having a temperature of 500–600°C. In fact, a temperature of 550°C has been used to denote maximum flaming regions by Bullen and Thomas (1979) and Chow and Han (2009). Taking 550°C as flame surface temperature, the spiral flame surface of 0.46 m fuel diameter agrees well with the experimental pattern. The 6 stages of fire whirl from generation to extinction are validated by comparing the experimental and simulated flame phases (Table 2).

Stage I simulated pattern is different from the experimental one due to assuming a linearly increasing HRR in the CFD input. Stage II simulated pattern inclines to the gap because of the air distribution. Gas temperature rises due to combustion and leads to stronger buoyancy with increased entrained air velocity. When the uneven velocity field is coupled with the buoyancy field, the flame starts to transit to IFW in Stage III. As the coupled field becomes steady, an inclined IFW (Stage IV) and a stable IFW (Stage V) are then formed.

CFD-FDS results for streamline is shown in Fig. 8(a). IFW of SW-L trends to be more slender. The streamline of larger fuel diameter is more concentrated and higher than the others, which means that it has stronger and steady airflow. Spiral streamlines are observed and air is mainly entrained from the base of gap. The lower part of the flame swirls more strongly. As height increases, the swirling streamline decays. The top views of the velocity vectors across flame base are shown in Fig. 8(b). A larger fuel diameter leads to stronger fire whirl.

## 5. Temperature

An ordinary pool fire is divided into the flame region, intermittent region and plume region as in McCaffrey (1979). The centerline temperature varies with height as

$$\frac{2g\Delta T}{T_0} = k^2 \left(\frac{z}{Q}\right)^\eta \quad (12)$$

The characteristic region of flame corresponds to  $z/Q^{2/5}$  and comparisons between an ordinary pool fire and an IFW are shown in Table 4. The IFW flame region and intermittent region are longer than those in a pool fire. Fig. 9 shows the experimental and simulated temperature distribution comparing with McCaffrey pool fire centerline temperature (McCaffrey, 1979). Similar empirical formula is applicable to an IFW too. It can be seen that for the pool fire flame region the average temperature of centerline is nearly constant, but falls in the intermittent region to about 320°C. However, the IFW average temperature rises a little in the flame region. This is because stronger fuel vaporization and air entrained at lower part consume more heat. At the end of the intermittent region, the centerline temperature falls to 490°C, significantly higher than that of pool fire. Thus, one would expect taking 550°C as the flame surface is appropriate. Taking 550°C as the flame surface temperature, in the three simulated cases, the flames height is 1.7 m, 2.25 m and 3.15 m respectively. Photographs taken by Bullen and Thomas (1979) during the experiments suggest that this might underestimate the height by ~10%. Experimental results are 1.85 m, 2.25 m and 3.2 m, indicating good matching with results of simulation.

In Fig. 10, Tree D simulated temperature is higher than the experimental temperature while Tree E and F are not. Usually simulated results trend to overestimate temperature, but strong entrained air current at the base (Fig. 8 (a)) would result in a lower simulated temperature.

## 6. Tangential and Axial Velocity

Variation of tangential velocity along the radial length at different height (0.1 m, 0.3 m, 0.5 m and 0.8 m above the surface of fire pool) for the three cases are shown in Fig. 11. Trends of the four curves in the three cases are similar. The maximum tangential velocity is found on the flame surface, and the radial distance of maximum tangential velocity is equal to the vortex core radius in general. The vortex core radius is very close to the fuel pool radius.

Fig. 12 is the vertical distribution of tangential velocity at different radial distances. The tangential velocity is larger at pool radius (vortex core radius) than at other vertical line in or out the IFW, which indicates that air swirls most strongly at the pool radius surface. Also, the tangential velocity fluctuates around  $z=0$  at the centerline of the fire whirl. At each radius surface outside the IFW, tangential velocity starts to rise to a maximum at the flame base, and after decreasing a little bit, the tangential velocity maintains stable with height. The curves reach the peak at 1.36 m, 1.6 m, 0.8 m, and  $\Omega_{\max} = 3.6 \text{ m/s}, 3.9 \text{ m/s}, 4.8 \text{ m/s}$ .

Variation of the centerline average velocity of fire whirl with height is shown in Fig. 13. It is observed that the centerline axial velocity increases rapidly with height due to increasing density difference and pressure gradient difference until its maximum value is reached. The maximum velocity appears at the average height of the flame. Comparing with McCaffrey's ordinary pool fire axial velocity fitted line, the IFW simulated data are not a function of  $Q^{2/5}$  any more. This is because pool fire velocity consists of radial and axial velocity but not tangential velocity. The tangential velocity has an increasing effect on the axial velocity. The IFW axial velocity increases more slowly than in pool fire because of the lower temperature distribution at the base of the flame due to stronger fuel vaporization. However, the maximum

axial velocity of IFW is much larger than the maximum axial velocity of a turbulent pool fire with the same diameter at the position higher than 0.6 m.

## **7. Conclusion**

Characteristics of an IFW were studied by both experimental and numerical methods. The temperature (average and time dependent), burning rate, IFW height and diameter were measured. With SGS Smagorinsky CFD-FDS simulation, the simulated results agree well with the experimental results in flame patterns, velocity (vertical and tangential), vortex core radius. Major results are summarized below.

- (1) Circumferential non-uniform density difference and baroclinic gradient due to buoyancy contribute to tangential current generation. Thus IFW forms more easily with larger HRR.
- (2) Single corner gap IFW character development process can be divided into 6 stages. In each stage the relationship between the vertical transient temperature and flame shape is summarized. Good agreements of experimental and simulated flame surface are achieved.
- (3) Comparison between average vertical temperature of IFW and pool fire is studied. IFW has longer flame region and intermittent region. Empirical equation for IFW vertical temperature is given.

## **Funding**

This study was sponsored by the National Natural Science Foundation of China (No. 11402061). The work described in this paper was also partially supported by a grant from the Research Grants Council of the Hong Kong Special Administrative Region, China for the

project “A study on electric and magnetic effects associated with an internal fire whirl in a vertical shaft” (Project No. PolyU 15206215) with account number B-Q47D.

## References

- [1] Soma, S. and Saito, K., Reconstruction of Fire Whirls using Scale Models, *Combust Flame*, vol. **86**, no. 3, pp. 269-284, 1991.
- [2] Emmons, H.W. and Ying S.J., The Fire Whirl, *Proceedings of the 11th international Symposium on Combustion*, Berkeley, CA, 14-20 August 1996, Pittsburgh, PA: Combustion Institute, pp. 475-488, 1996.
- [3] Satoh, K. and Yang, K.T., Experimental Observations of Swirling Fires, *AMSE Heat Transfer Division*, vol. **335**, pp. 393-400, 1996.
- [4] Satoh, K. and Yang, K.T., 1998. Experiments and Numerical Simulations of Swirling Fires due to 2×2 Flames in a Channel with Single Corner Gap, *Proceedings of ASME International Mechanical Engineering Congress and Exposition, ASME Heat Transfer Division*, 15-20 November 1998, Anaheim, CA, vol. **2**, pp. 120-127, 1998.
- [5] Satoh, K. and Yang, K.T., Measurements of Fire Whirl from a Single Flame in a Vertical Square Channel with Symmetrical Corner Gaps, *Proceedings of ASME International Mechanical Engineering Congress and Exposition, ASME Heat Transfer Division*, 14-19 November 1999, Nashville, TN, vol. **364**, pp. 167-173, 1999.
- [6] Yu, Hanyuan and Guo, Song, Study on the Influence of Air-Inlet Width on Fire Whirls Combustion Characteristic, *Procedia Eng.*, vol. **62**, pp. 813-820, 2013.
- [7] Zou, G.W. and Chow, W.K., Generation of an Internal Fire Whirl in an Open Roof Vertical Shaft Model with a Single Corner Gap, *J. Fire Sci.*, vol. **33**, no. 3, pp. 35-42, 2015.
- [8] Lei, Jiao and Liu, Naian., Experimental Research on Flame Revolution and Precession of Fire Whirls, *Proc. Combust. Inst.*, vol. **34**, no. 2, pp. 2607-2615, 2013.

- [9] Lei, Jiao and Liu, Naian., Temperature, Velocity and Air Entrainment of Fire Whirl Plume: A Comprehensive Experimental Investigation, *Combust. Flame*, vol. **162**, no. 3, pp. 745-758, 2015.
- [10] Lei, Jiao, Liu, Naian and Tu, Ran., Flame Height of Turbulent Fire Whirls: A model Study by Concept of Turbulence Suppression, *Proc. Combust. Inst.*, vol. **36**, pp. 3131-3138, 2017.
- [11] Chuah, K.H., Kuwana, K. and Saito, K., Modeling a Fire Whirl Generated Over a 5-cm-Diameter Methanol Pool Fire, *Combust. Flame*, vol. **156**, pp. 1828-1833, 2009.
- [12] Liu, S.L. and Chow, W.K., A Review on Numerical Simulation of Turbulent Flow, *International Journal on Architectural Science*, vol. **3**, no. 2, pp. 77-102, 2002.
- [13] Ma, T. and Quintiere, J., Numerical Simulation of Axi-Symmetric Fire Plumes: Accuracy and Limitations, *Fire Saf. J.*, vol. **38**, no. 5, pp. 467-492, 2003.
- [14] Murakami, S., Overview of Turbulence Models Applied in CWE-1997, *J. Wind Eng. Ind. Aerodyn.*, vol. **74**, pp. 1-24, 1998.
- [15] Zhang, W. and Chen, Q.Y., Large Eddy Simulation of Indoor Airflow with a Filtered Dynamic Subgrid Scale Model, *Int. J. Heat Mass Transfer*, vol. **43**, no. 17, pp. 3219-3231, 2000.
- [16] Jiang, Y. and Chen, Q.Y., Study of Natural Ventilation in Buildings by Large Eddy Simulation, *J. Wind Eng. Ind. Aerodyn.*, vol. **89**, no. 13, pp. 1155-1178, 2001.
- [17] Satoh, K. and Yang, K.T., Simulation of Swirling Fires Controlled by Channeled Self-generated Entrainment Flows, *Fire Safety Science - Proceedings of the 5th International Symposium*, International Association for Fire Safety Science, pp. 208-216, 1997.
- [18] Chow, W.K., Dang, J.F., Gao, Y. and Chow, C.L., Dependence of Flame Height of Internal Fire Whirl in a Vertical Shaft on Fuel Burning Rate in Pool Fire, *Appl. Therm. Eng.*, vol. **121**, pp. 712-720, 2017.

- [19] Snegirev, A.Yu. and Marsden J.A., Numerical Studies and Experimental Observations of Whirling Flames, *Int. J. Heat Mass Transfer*, vol. **47**, pp. 2523-2539, 2004.
- [20] McGrattan, K.B., and Forney, G.P., Fire Dynamics Simulator (Version 4) - User Guide. NIST Special Publication 1019, National Institute of Standards and Technology, pp. 1-90, 2004.
- [21] McGrattan, K.B., Fire Dynamics Simulator (Version 4) - Technical Reference Guide, NIST Special Publication 1018, National Institute of Standards and Technology, pp. 1-85, 2004.
- [22] Zhou, X., Luo, K.H. and Williams, J.J.R., Numerical Studies On Vortex Structures In The Near-Field Of Oscillating Diffusion Flame, *Heat Mass Transfer*, vol. **137**, pp.110-161, 2001.
- [23] Warrantz, U., Maas, U. and Debbie, R.W., *Combustion*, Berlin: Springer-Verlag, 1996.
- [24] Zhang, W., Hamer, A., Klassen, M. and Carpenter, D., Turbulence Statistics in a Fire Room Model by Large Eddy Simulation, *Fire Saf. J.*, vol. **37**, no. 8, pp. 721-752, 2002.
- [25] Cheung, S.C.P. and Yeoh, G.H., A Fully-coupled Simulation of Vertical Structures in a Large-scale Buoyant Pool Fire, *Int. J. Therm. Sci.*, vol. **48**, pp. 2187-2202, 2009.
- [26] Wang, H.Y., Numerical Study of Under-ventilated Fire in Medium-scale Enclosure, *Build. Environ.*, vol. **44**, no. 6, p. 1215-1227, 2009.
- [27] Zukoski, E.E., Kubota, T. and Cetegen, B., Entrainment in fire plumes, *Fire Saf. J.*, vol. **3**, no. 3, pp. 107-121, 1981.
- [28] Bullen, M.L. and Thomas, P.H., Compartment Fires with Non-cellulosic Fuels, *Proc. Combust. Inst.*, vol. **17**, pp. 1139-1148, 1979.
- [29] Chow, W.K. and Han S.S., Experimental Investigation on Onsetting Internal Fire Whirls in a Vertical Shaft, *J. Fire Sci.*, vol. **27**, no. 6, pp. 529-543, 2009.
- [30] McCaffrey, B.J., Purely Buoyant Diffusion Flames: Some Experimental Results. NBSIR

79-1910, National Bureau of Standards, Gaithersburg, Maryland, pp. 10-16, 1979.

HTR\_SS LiIFW-16B-1p

## List of Tables

Table 1. Experimental parameters and results

Table 2. Experimental and simulated flame phase of SW-L

Table 3. Grids of different cases

Table 4. Parameter differences between pool fire and IFW

## List of Figures

Fig. 1: Vertical shaft

Fig. 2: Central gas temperatures under 0.8 m

Fig. 3: Radial gas temperatures at different heights

Fig. 4: Transient fuel mass

Fig. 5: Simulation geometry of model and grid

Fig. 6: Input HRRs in simulations. The horizontal section corresponding to experimental stable fire whirl stage HRR.  $\bar{Q}_{in}$  =99.5 kW, 168 kW and 440.5 kW respectively.

Fig. 7: SW-L simulated results. (a)Temperature varied 20-870 °C (b)Pressure varied -90~2 Pa. (c) Velocity varied 0~8.5 m/s. (d)  $v$  varied -5.5~4.5 m/s. (e)  $w$  varied -1.3~8.7 m/s.  $t=150s$ . Blue represents small value and red represents large value.

Fig. 8: Stage V streamline (a) and velocity vector (b) at  $z = 0.5$  m

Fig. 9: Centerline excess temperature versus  $z/Q^{2/5}$

Fig. 10: Comparisons between experimental and numerical radial temperatures with 0.46 m diameter fire

Fig. 11: Tangential velocity versus radius at different height

Fig. 12: Variation of tangential velocity versus height at different radial location. From top to bottom,  $r = 0$ ,  $r = r_m$ ,  $r = r_m + 0.2$ ,  $r = r_m + 0.5$

Fig. 13: Average centerline velocity

Table 1. Experimental parameters and results

Label	Fuel diameter (m)	Mass (kg)	Fuel depth (cm)	HRR estimated		Fuel burning rate		Burning time (s)	Maximum flame height (m)	Mean flame height (m)
				from burning rate (kW)		(gs <sup>-1</sup> )				
				Mean( $\bar{Q}$ )	Stage V( $Q$ )	Mean	Stage V			
SW-S	0.2	0.91	4	103.4	125.1	2.8	3.4	330	1.85	1.46
SW-M	0.26	1.53	4	173.0	213.4	4.7	5.8	327	2.25	1.81
SW-L	0.46	4.81	4	441.6	552.0	12.0	15.1	401	3.2	2.5

Table 2. Experimental and simulated flame phase of SW-L






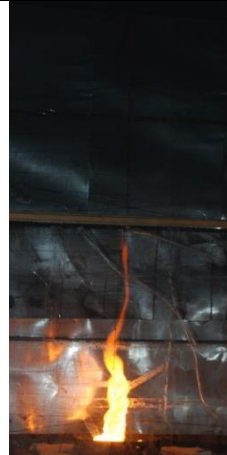
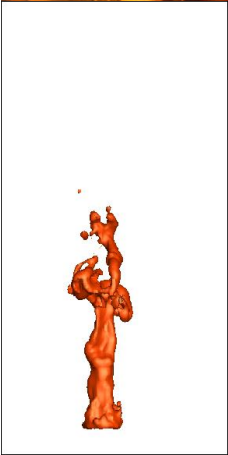
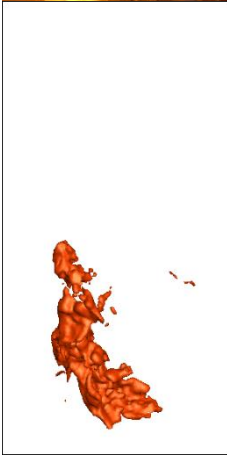
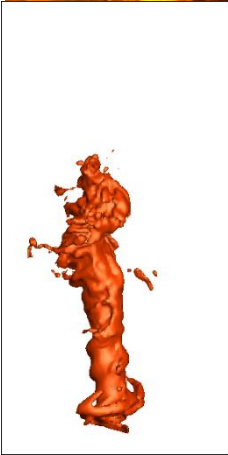
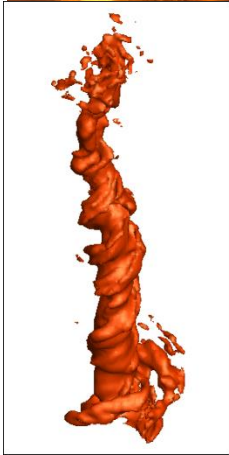
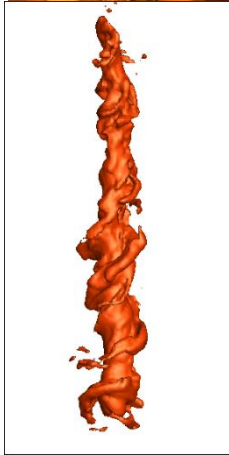
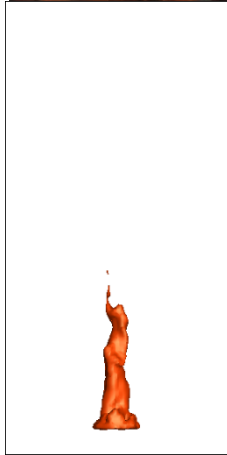
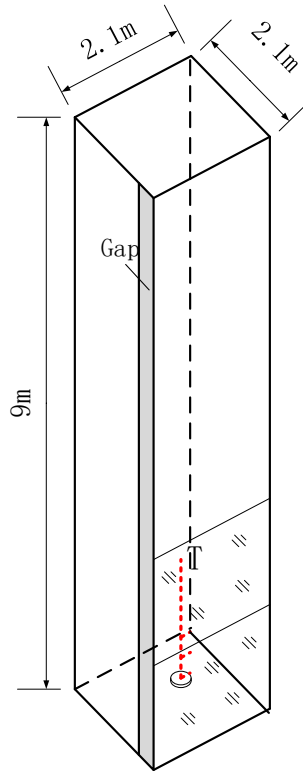
Stage	I	II	III	IV	V	VI
Flame phase	Ordinary pool fire	Inclined pool fire	Transition fire	Inclined fire whirl	Straight fire whirl	Weak straight fire whirl
Experi- mental patterns						
						

Table 3. Grids of different cases

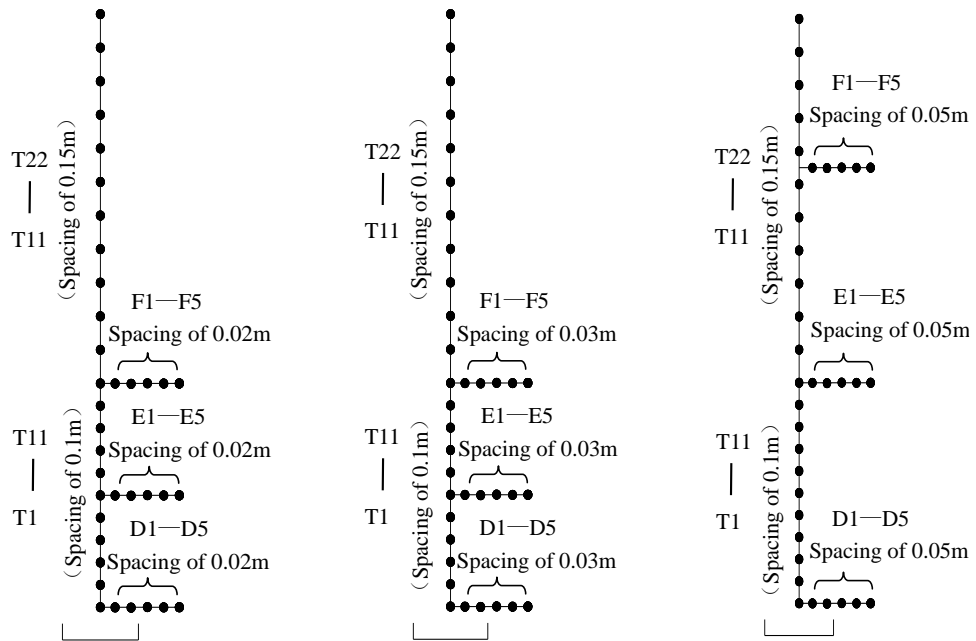
Simulation Number	$q$ (kW)	$D^*$	Grid size (m)	Grid size in flame zone (m)
SW-S	125.1	0.35	0.035	0.03
SW-M	213.4	0.45	0.045	0.03
SW-L	552	0.65	0.065	0.05

Table 4. Parameter differences between pool fire and IFW

Region	Pool fire			IFW		
	$k$	$\eta$	$z / Q^{2/5}$ (m/kW <sup>2/5</sup> )	$k$	$\eta$	$z / Q^{2/5}$ (m/kW <sup>2/5</sup> )
Flame	7.5m <sup>1/2</sup> /s	0	<0.08	7.7 m <sup>1/2</sup> /s	0.3	<0.1
Intermittent	2.1m/kW <sup>1/5</sup> ·s	-1	0.08-0.2	4.4 m/kW <sup>1/5</sup> ·s	-0.42	0.1-0.25
Plume	1.2 m/kW <sup>1/3</sup> ·s	-5/3	>0.2	2 m/kW <sup>1/3</sup> ·s	-1.58	>0.25



(a) The rig



(i) 0.2 m diameter

(ii) 0.26 m diameter

(iii) 0.46 m diameter

(b) Temperature measurement points for different gasoline pool diameters

Fig. 1: Vertical shaft

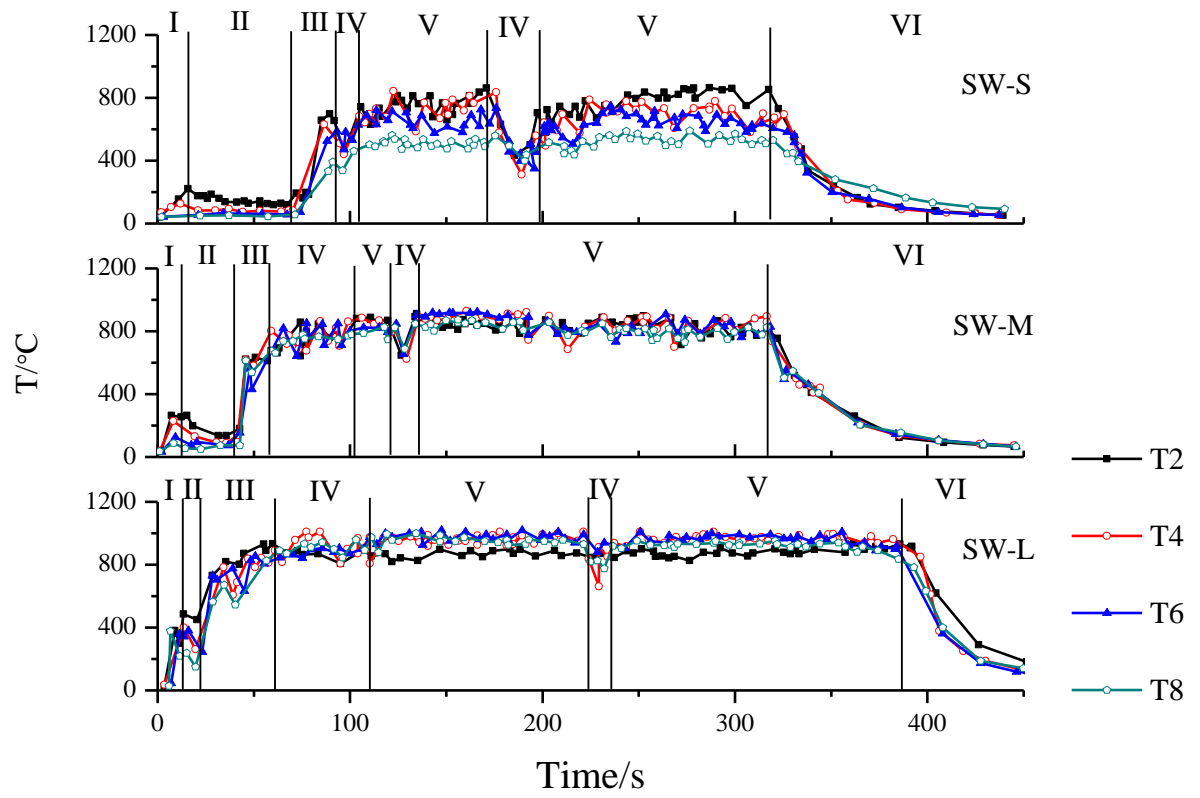


Fig. 2: Central gas temperatures under 0.8 m

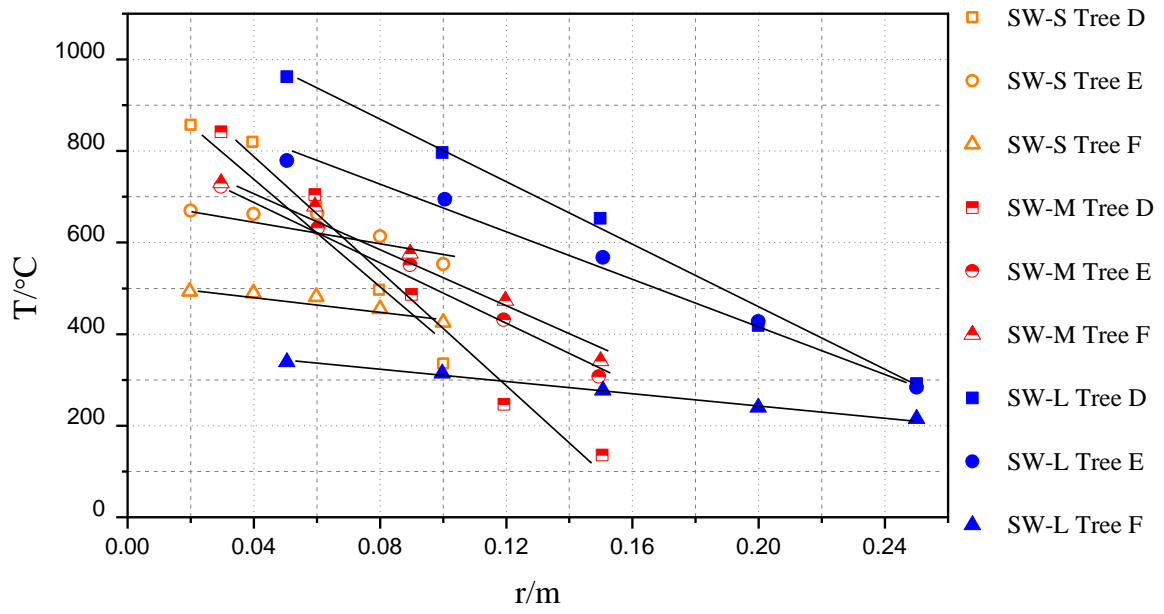


Fig. 3: Radial gas temperatures at different heights

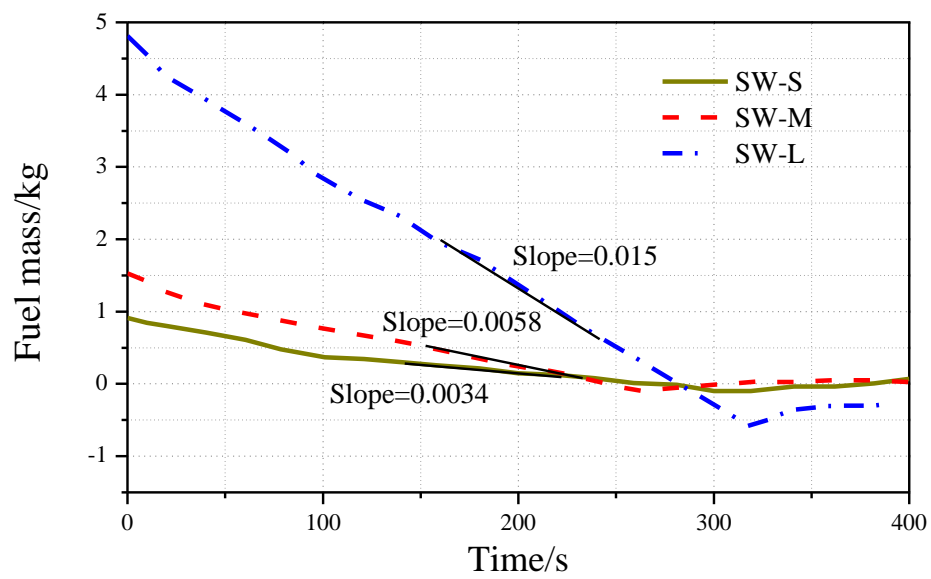


Fig. 4: Transient fuel mass

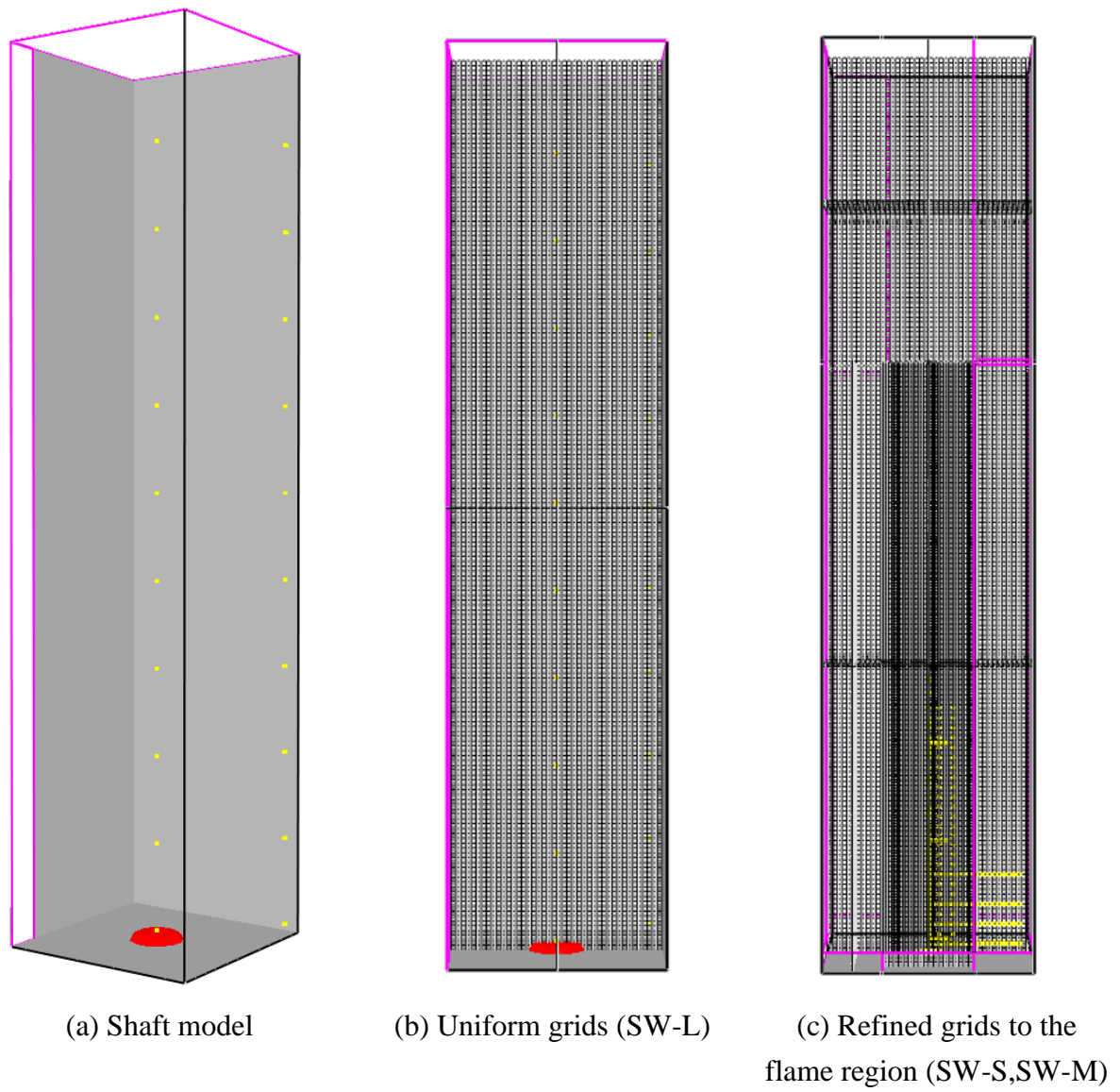


Fig. 5: Simulation geometry of model and grid

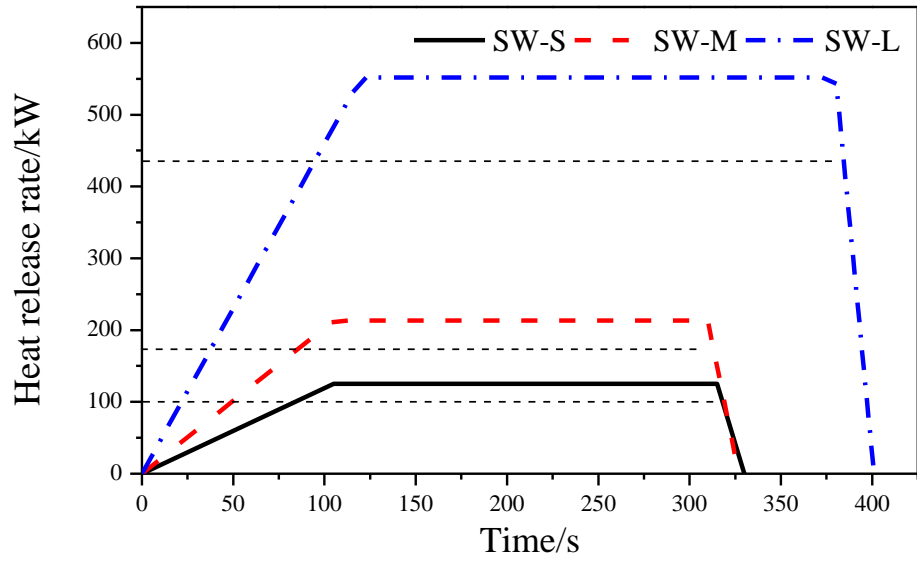


Fig. 6: Input HRRs in simulations. The horizontal section corresponding to experimental stable fire whirl stage HRR.  $\bar{Q}_{in}$  =99.5 kW, 168 kW and 440.5 kW respectively.

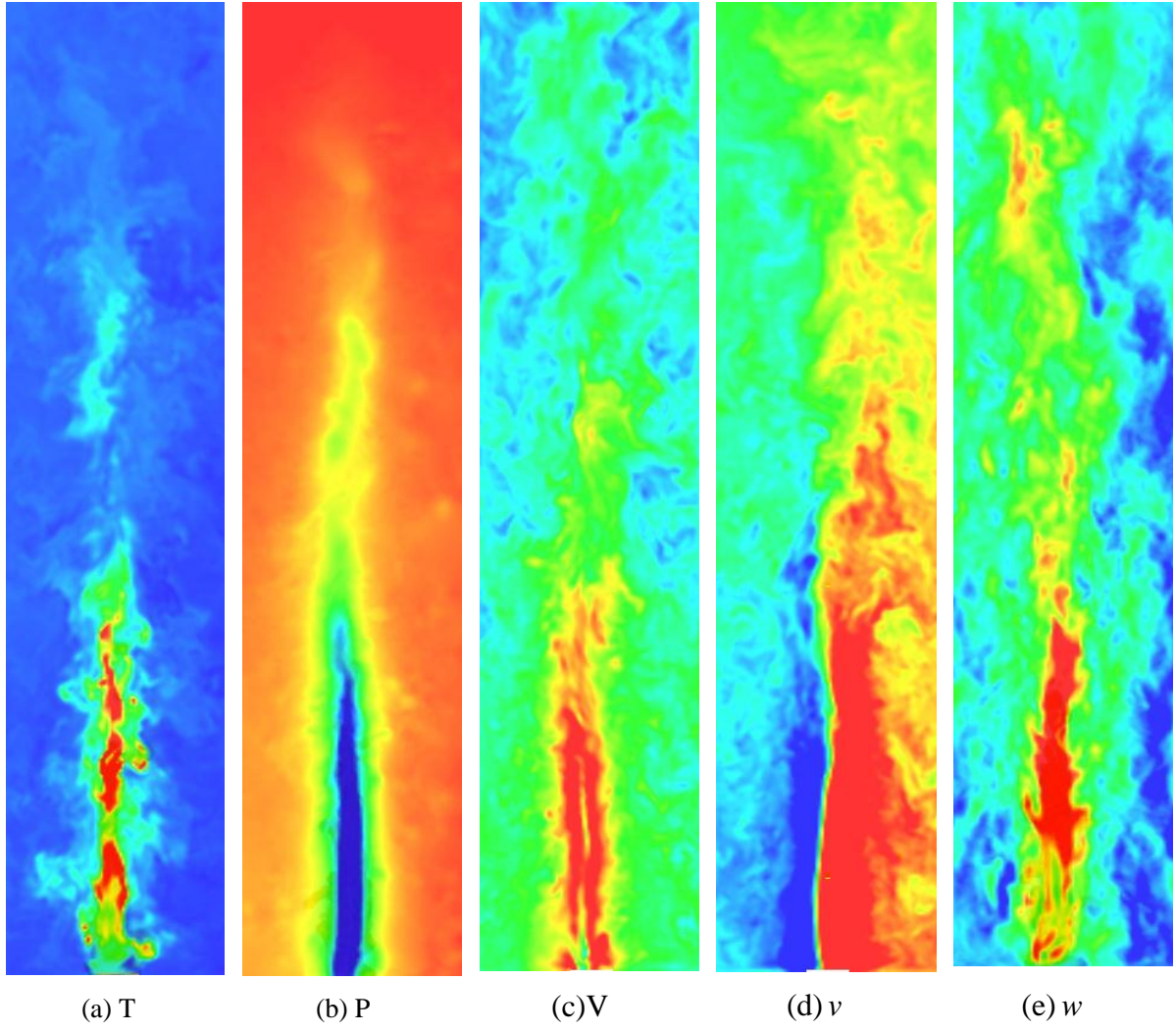
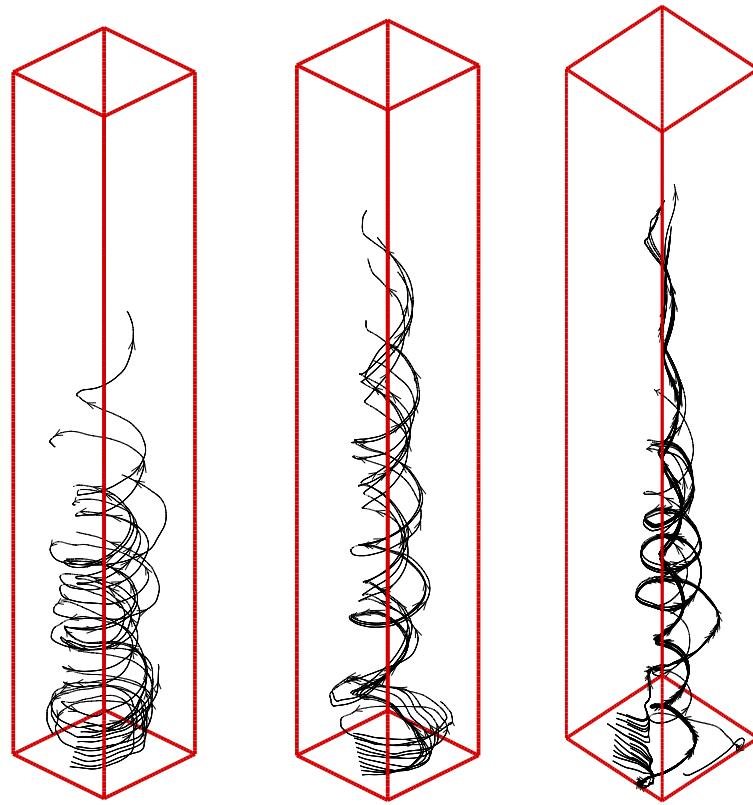


Fig. 7: SW-L simulated results. (a)Temperature varied 20-870  $^{\circ}C$  (b)Pressure varied -90~2 Pa. (c) Velocity varied 0~8.5 m/s. (d)  $v$  varied -5.5~4.5 m/s. (e)  $w$  varied -1.3~8.7 m/s.  $t=150s$ . Blue represents small value and red represents large value.

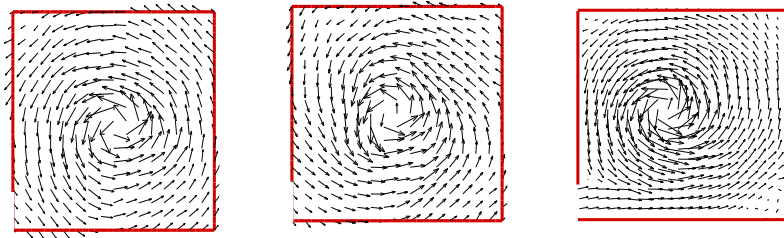


(i) SW-S

(ii) SW-M

(iii) SW-L

(a) Streamline of three IFWs



(i) SW-S

(ii) SW-M

(iii) SW-L

(b) Velocity vector of three IFWs

Fig. 8: Stage V streamline (a) and velocity vector (b) at  $z = 0.5$  m

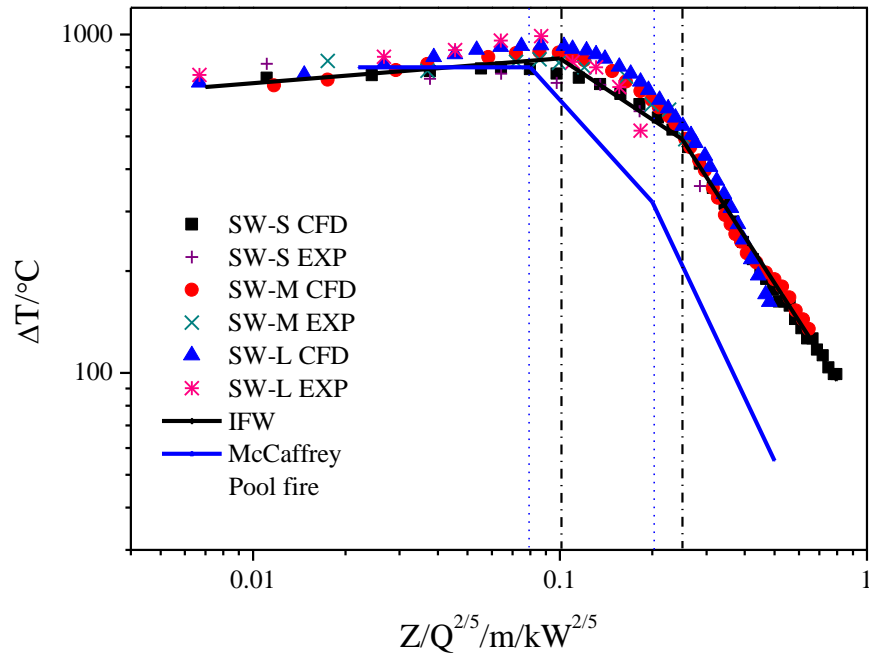


Fig. 9: Centerline excess temperature versus  $z/Q^{2/5}$

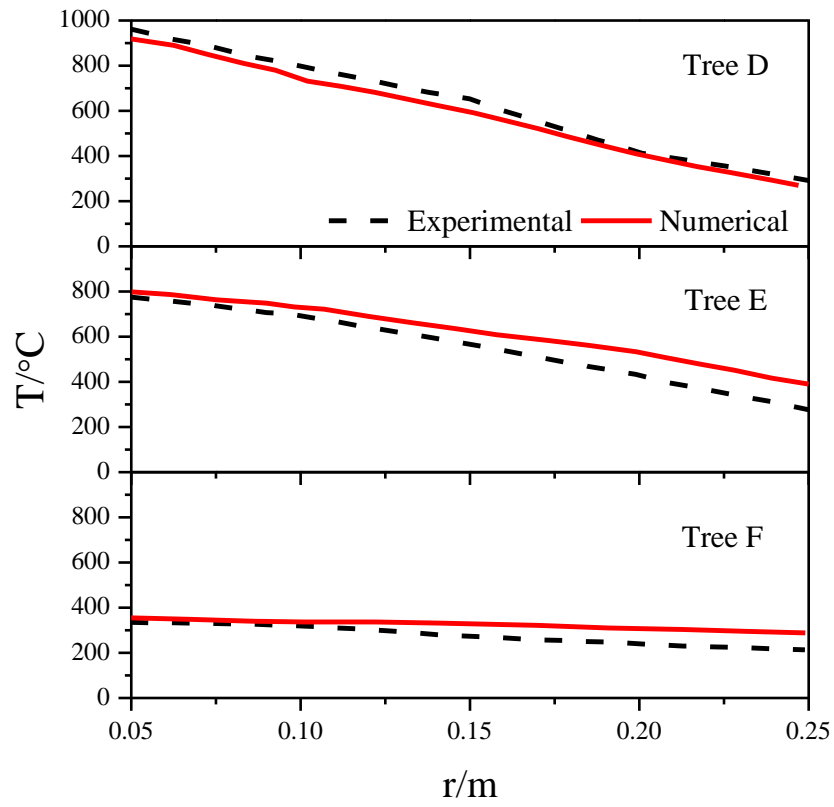


Fig. 10: Comparisons between experimental and numerical radial temperatures with 0.46 m diameter fire

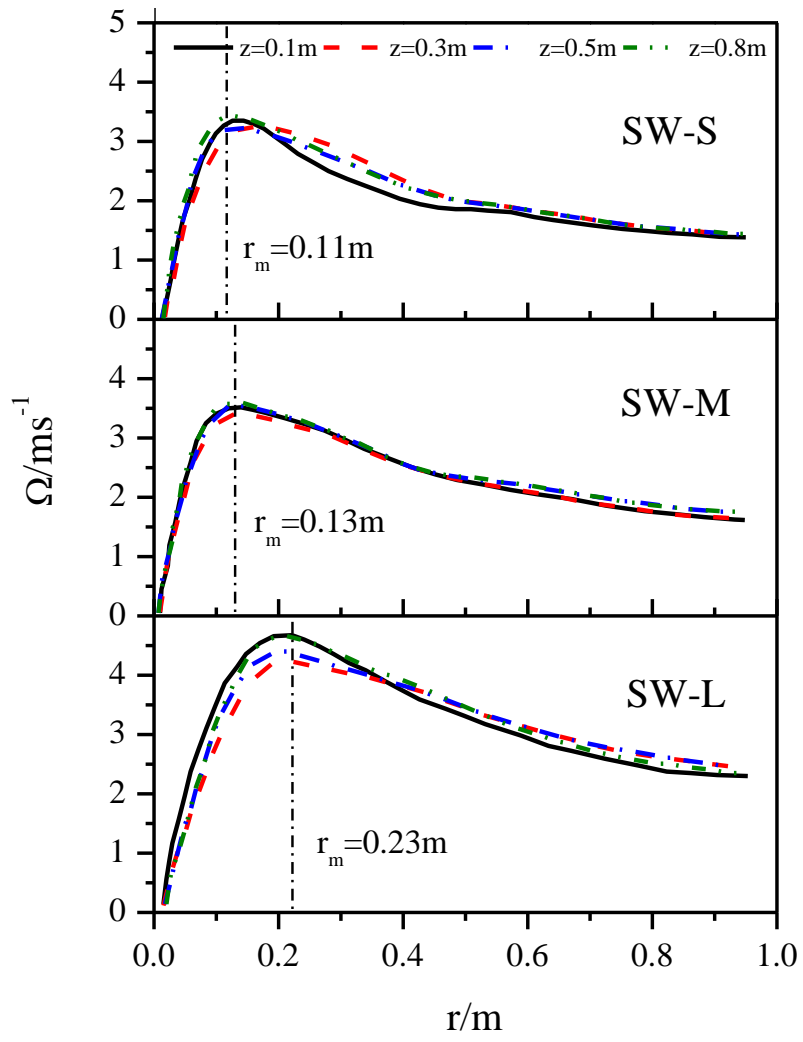


Fig. 11: Tangential velocity versus radius at different height

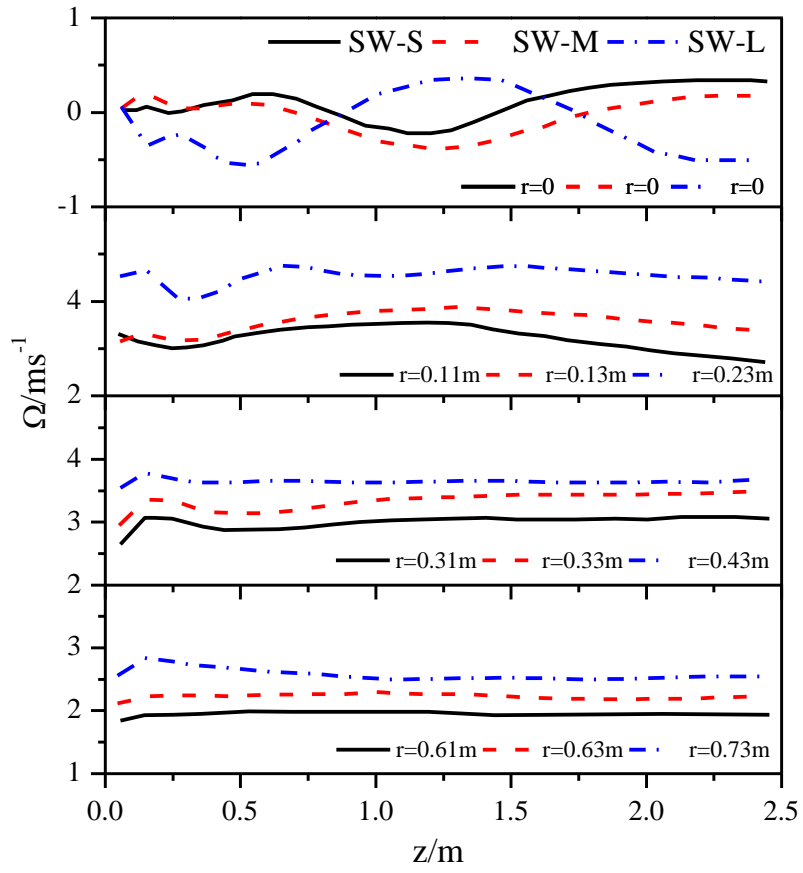


Fig. 12: Variation of tangential velocity versus height at different radial location. From top to bottom,  $r = 0$ ,  $r = r_m$ ,  $r = r_m + 0.2$ ,  $r = r_m + 0.5$ .

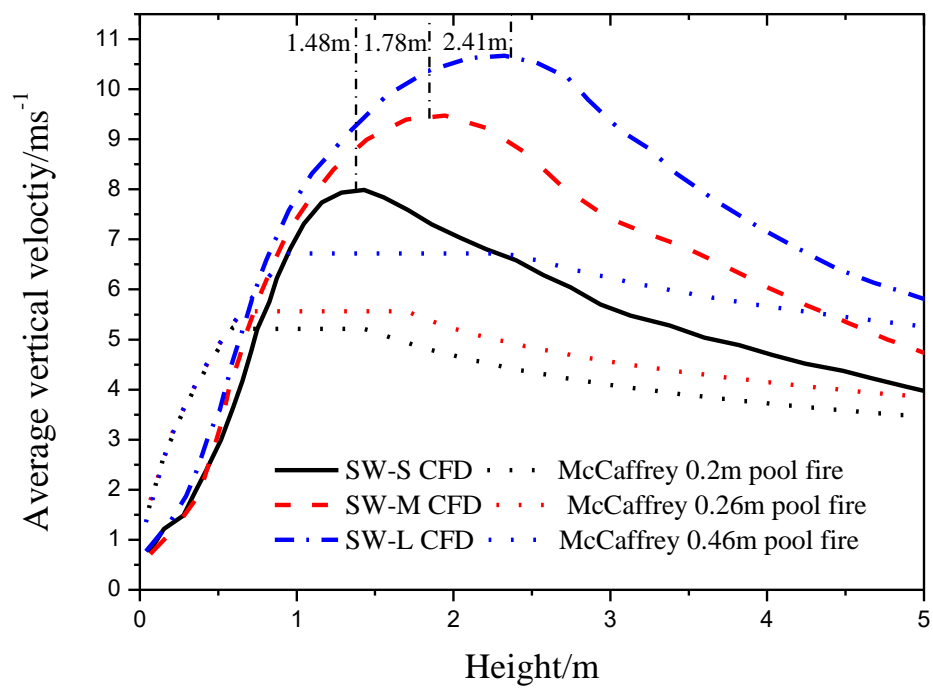


Fig. 13: Average centerline velocity